Formation of ions by high-energy photons

E. G. Drukarev,[1] A. I. Mikhailov,[1] I. A. Mikhailov,[1] Kh. Yu. Rakhimov,[2] and W. Scheid[3]
[1]*Petersburg Nuclear Physics Institute, Gatchina, St. Petersburg 188300, Russia*
[2]*Heat Physics Department of the Uzbek Academy of Sciences, Tashkent 700135, Uzbekistan*
[3]*Justus-Liebig-Universität Giessen, Giessen 35392, Germany*
(Received 28 October 2006; published 26 March 2007)

We calculate the electron energy spectrum of ionization by a high-energy photon, accompanied by creation of an e^-e^+ pair. The total cross section of the process is also obtained. The asymptotics of the cross section does not depend on the photon energy. At the photon energies exceeding a certain value ω_0 this appears to be the dominant mechanism of formation of the ions. The dependence of ω_0 on the value of nuclear charge is obtained. Our results are consistent with experimental data.

DOI: 10.1103/PhysRevA.75.032717 PACS number(s): 32.80.Fb

I. INTRODUCTION

In the present paper we calculate the cross sections σ for formation of ions in interactions of the high-energy photons with atoms. We calculate also the distribution $d\sigma/d\varepsilon$ for the process in which the final state contains an ion and an electron with energy ε. We consider the high-energy asymptotics of these characteristics, i.e., we consider the photon energies

$$\omega \gg m, \tag{1}$$

with m standing for the electron mass at rest (we employ the system of units with $\hbar=c=1$). We shall include only the lowest terms of expansion in ω^{-1} in our calculations.

The simplest mechanism for formation of ions is the photoionization (photoeffect), in which the final state consists of ion and the continuum electron. It is also known that while the energies increase, the Compton scattering on the bound electron dominates. Recently, Ionescu *et al.* [1] noted that at still higher energies ions are produced mainly being accompanied by creation of electron-positron pairs and provided estimates for the cross section σ.

Here we carry out the calculations for the distributions $d\sigma/d\varepsilon$ and for the cross section σ. We focus on the case of not very large values of nuclear charge

$$(\alpha Z)^2 \ll 1, \tag{2}$$

adding, however, analysis of the case, when $(\alpha Z)^2$ is not considered as a small parameter. When the unequality (2) is true, we can separate three scales of the electron kinetic energies ε. Besides the characteristic values of ω and m, the third one is the electron binding energy I_b. For K shell in the hydrogenlike approximation $I_b=I=\eta^2/2m$, with $\eta=m\alpha Z$.

We demonstrate that for the energies $\varepsilon \sim m$ the distribution $d\sigma/d\varepsilon$ is determined by the vacuum assisted mechanism. The ionized electrons can be distinguished from those of the e^-e^+ pair since the latter carry mostly energies $\varepsilon_i \sim \omega \gg m$. We show how the distribution can be presented in terms of the pair creation on a free electron at rest. We show also that at these values of the electron energies the distribution does not depend on the details of atomic structure. At $\varepsilon \ll m$ the distribution behaves as ε^{-1}. This means that in order to calculate the cross section σ one has to include the region $\varepsilon \sim I$ which should be treated separately. We show that in the asymptotics (1) the cross section reaches a constant value and calculate it.

In Sec. II we present general equations. In Sec. III we calculate distribution $d\sigma/d\varepsilon$ for $\varepsilon \gg I$. In Sec. IV we calculate this distribution for $\varepsilon \sim I$. In Sec. V we carry out matching of the energy distributions in the two regions. In Sec. VI we calculate the cross section of ion production σ and compare results of our calculations with experimental data. We summarize in Sec. VII.

II. NOTATIONS AND GENERAL FORMULAS

In all the processes considered in the paper an electron is removed from the atom to continuum. It will be instructive to consider simultaneously a similar process on the free electron at rest. For the latter case we denote the four-momenta of the electrons as $p_{1,2}$ with the time component $p_{10}=m$ and $\mathbf{p}_1=\mathbf{0}$. We denote four-momenta of the electron and positron of the created e^-e^+ pair as p_e and p_p correspondingly. For each $p_i(i=e,p,1,2)$ the total energy is $E_i=\sqrt{m^2+\mathbf{p}_i^2}$, while kinetic energies are $\varepsilon_i=E_i-m$. The four-momentum of the incoming photon is k, while for its three-dimension momentum we can write $|\mathbf{k}|=\omega$.

In the pair production on the nucleus the latter accepts linear momentum

$$\mathbf{q}=\mathbf{k}-\mathbf{p}_e-\mathbf{p}_p. \tag{3}$$

In the pair production on free electron momentum (3) is transferred to the latter. In pair production on the bound electron momentum

$$\mathbf{Q}=\mathbf{q}-\mathbf{p}_2 \tag{4}$$

is transferred to the residual ion.

The cross section for pair creation in the field of the nucleus was first calculated by Bethe and Heitler [2]. It can be represented as

$$d\sigma_{\mathrm{BH}}=\frac{\pi}{\omega}|F_{\mathrm{BH}}(\omega,p_e,p_p)|^2\delta(\omega-E_e-E_p)d\Gamma, \tag{5}$$

with the phase volume $d\Gamma=[d^3p_e/2E_e(2\pi)^3]\times[d^3p_p/2E_p(2\pi)^3]$.

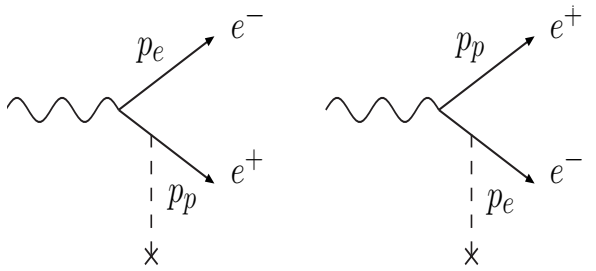

FIG. 1. Feynman diagrams describing creation of an e^-e^+ pair in the field of the nucleus by the photon. Wavy line shows the photon, solid lines show electron and positron, and dashed line stands for the interactions between the created pair and the nucleus.

At $\omega \gg m$ it is convenient to present momenta p_i $(i=e,p)$ as $p_i=(E_i,p_{iz},\mathbf{p}_{it})$ with the axis z directed along photon momentum $\mathbf{k}$. The lower index t denotes the components, which are orthogonal to $\mathbf{k}$. The energy distributions are determined by small $p_{it} \sim m$ $(i=e,p)$ [2,3] with q being determined by Eq. (3). Thus presenting

$$E_i = |p_{iz}| + \frac{m^2 + p_{it}^2}{2|p_{iz}|}, \tag{6}$$

we find that the longitudinal component of the recoil momentum $\mathbf{q}$ is m/ω times smaller than the transverse one. Hence we can write

$$\mathbf{q} = -\mathbf{p}_{et} - \mathbf{p}_{pt}. \tag{7}$$

For the pair creation in the field of the bound electron the cross section is

$$d\sigma = \frac{\pi}{\omega}|F(\omega,p_e,p_p,p_2)|^2 \delta(\omega - E_e - E_p - E_2 + m - I_b) d\Gamma_b, \tag{8}$$

with F being the amplitude of the process, while $d\Gamma_b = d\Gamma[d^3p_2/2E_2(2\pi)^3]$ with I_b standing for the ionization potential of the bound state.

To avoid writing complicated expressions which describe the third order amplitudes F_{BH} and F we present them by the Feynman diagrams, following [1]. The pair creation in the field of the nucleus is shown by the diagrams of Fig. 1. The pair creation on the bound electron is shown by the diagrams of Fig. 2. The possible permutations of the final state electrons should be added. Figures 2(a) shows creation of pairs by the photon with further scattering on the bound electron. In Fig. 2(b) the photon is initially absorbed by the bound electron with further radiation of a photon which creates the electron-positron pair.

III. FAST IONIZED ELECTRONS

Here we consider the case of fast ionized electrons with the energies

$$\varepsilon_2 \gg I, \tag{9}$$

with I being the ionization potential of the K shell electron. We focus on the energies $\varepsilon_2 \ll \omega$, since these values provide the leading contribution to the cross section.

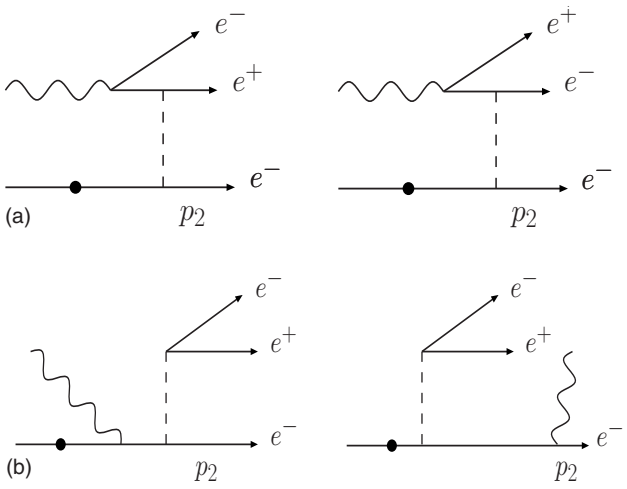

FIG. 2. Feynman diagrams describing creation of an e^-e^+ pair accompanied by removal of the bound electron (denoted by dark blob) to continuum state with asymptotic momentum p_2. Other notations are the same as in Fig. 1.

The electrons with the energies $\varepsilon_2 \ll \omega$ can come from e^-e^+ pairs and also can be caused by removal of the bound electrons to continuum. In the former case the distribution $d\sigma/d\varepsilon$ drops as ω^{-1} [2,3]. We shall see that in the latter case it does not depend on ω. Thus the electrons with energies $\varepsilon_2 \ll \omega$ are mainly those which are knocked out from the atom.

Momentum Q should be transferred to residual ion. It can be transferred by the initial state bound electron or by final state continuum lepton (electron or positron). It is known [3] that each interaction of the continuum electron with residual ion provides a factor $\alpha Z E_i/p_i$. On the other hand, in the bound state wave function momentum Q is compared to the bound state characteristic momentum η_b. The wave function reaches its largest values at $Q \sim \eta_b$, being strongly quenched at $Q \gg \eta_b$. Thus in the amplitude $F(p_i,Q)$ (with p_i denoting momenta of the outgoing electrons and that of positron) we can neglect Q everywhere except the bound state wave function. This enables us to tie the amplitude of the process on the bound electron with that on the free electron $F_0(p_i)$, known as triplet production. Such interpretation of the processes on the bound electrons reflects the ideas of Bethe [4] (see also analysis presented in [5]).

Assuming that the bound electron is described by a single-particle wave function $\psi(r)$ we can write for the amplitude of the pair creation on the bound electron

$$F(p_i,Q) = \psi_F(Q) F_0(p_i). \tag{10}$$

Here

$$\psi_F(Q) = \int d^3r\, \psi(r) \exp[-i(\mathbf{Q}\cdot\mathbf{r})] \tag{11}$$

is the Fourier transform of the wave function $\psi(r)$ also referred to as the wave function in momentum space. To simplify notations we shall omit the lower index F further.

Note that the outgoing electrons can be described by plane waves due to a small value $Q \ll m$ of momentum trans-

ferred to the nucleus. In other words, this is due to the existence of a kinematical region, where similar process on a free electron could take place. For example, there is no such kinematical region for the photoeffect, and the plane wave description for relativistic energies is not sufficient [3]. See a more recent discussion in [5].

Replacing d^3p_e by d^3Q in the phase volume we find for the cross section

$$d\sigma = \frac{\pi}{\omega}|F_0(\omega,p_e,p_p,p_2)|^2\delta(\omega - E_e - E_p - E_2 + m - I_b) \times \frac{1}{2E_e}\frac{d^3p_p}{2E_p(2\pi)^3}\frac{d^3p_2}{2E_2(2\pi)^3}|\psi(Q)|^2\frac{d^3Q}{(2\pi)^3}. \quad (12)$$

Neglecting I_b with respect to m and ω we find

$$d\sigma = d\sigma_0|\psi(Q)|^2\frac{d^3Q}{(2\pi)^3}, \quad (13)$$

with σ_0 being the cross section of the process on free electron. After integration over Q providing $\int|\psi(Q)|^2[d^3Q/(2\pi)^3]=1$ (normalization condition) we find the distributions $d\sigma$ to be equal to those of the process on the free electron.

The triplet production was much studied [6–10]. It was shown in [6], that in the considered region the diagrams of Fig. 2(b) as well as the exchange diagrams of Fig. 2(a) can be neglected. Analytical expression for the differential distribution integrated over the variables of the e^-e^+ pair was obtained in [7]. The leading term of expansion in powers of ω^{-1} for the distribution of the ionized electron can be written as

$$\frac{d\sigma}{d\varepsilon_2 d\Delta^2} = n_e\alpha^3 W(\varepsilon_2,\Delta^2). \quad (14)$$

Here $\Delta^2=(p_e+p_p)^2$, it can be expressed in terms of variables of the ionized electron as $\Delta^2=-2\varepsilon_2(\omega+m)+2\omega p_2 t_2$; $t_2=(\mathbf{k}\cdot\mathbf{p}_2)/\omega p_2$, and n_e stands for the number of the bound electrons in the atom. Evaluating Eq. (2.4) of [7] we find

$$W(\varepsilon_2,\Delta^2) = \frac{A(\varepsilon_2,\Delta^2)}{\varepsilon_2 B(\varepsilon_2,\Delta^2)}, \quad (15)$$

with

$$B(\varepsilon_2,\Delta^2) = (\Delta^2 + 2m\varepsilon_2)^2 \quad (16)$$

and

$$A(\varepsilon_2,\Delta^2) = 4\beta\left(1 - L + 4m\frac{[\Delta^2(m-4\varepsilon_2)] + L[2m^2(2\varepsilon_2+m) + \Delta^2(\varepsilon_2 - m)]}{B(\varepsilon_2,\Delta^2)}\right). \quad (17)$$

Here $\beta=[(\Delta^2-4m^2)/\Delta^2]^{1/2}$ and $L=(1/\beta)\ln[(1+\beta)/(1-\beta)]$.

Since the variable Δ^2 can be viewed as the squared energy of the e^-e^+ pair in their c.m. frame, we can write the limitation $\Delta^2 \geq 4m^2$. The upper limit is $\Delta^2=2m\omega$ [7]. The energy distribution can be obtained by integration of the differential cross section (15) over Δ^2 in these limits. The value is determined by the lower limit of Δ^2, providing

$$\frac{d\sigma}{d\varepsilon_2} = \frac{n_e\alpha r_e^2}{m}T_f\left(\frac{\varepsilon_2}{m}\right), \quad (18)$$

with $r_e=\alpha/m$, and (the lower index f comes from "fast")

$$T_f(x) = \frac{2}{x}\left[-\frac{x^3+x^2+2x-1}{x^2(2+x)^2} + \frac{2(2x^4+7x^3+16x^2+5x-3)}{3x^{5/2}(2+x)^{5/2}}\ln(\sqrt{x/2}+\sqrt{x/2+1}) - \frac{2(1-4x)}{15}{}_2F_1\left(2,4,\frac{7}{2},-\frac{x}{2}\right)\right]. \quad (19)$$

Here $x=\varepsilon_2/m$. The function $T_f(x)$ is shown in Fig. 3. At $x \ll 1$ we find

$$T_f(x) = \frac{14}{9}\frac{1}{x}. \quad (20)$$

Note that Eq. (19) is not true for $\varepsilon_2 \sim \omega$. Using Eq. (6) one can see that momentum transferred to the residual ion cannot be made as small as $Q \ll m$ if all the three final state leptons carry the energies $\varepsilon_i \sim \omega$.

Thus Eq. (19) is true for $I \ll \varepsilon_2 \ll \omega$. Since for $\varepsilon_2 \ll m$ the distribution behaves as ε_2^{-1}, the region $\varepsilon_2 \sim I$ provides a contribution of the same order of magnitude to the total cross section.

IV. SLOW IONIZED ELECTRONS

Now we consider the case $\varepsilon_2 \sim I$. In this case the outgoing electron carries momentum p_2 of the order of the binding momentum $\eta \ll m$. Thus momentum Q transferred to the residual ion can be as small as η only if momentum q transferred to the atom is also of the order of η. Hence the amplitude of the ionization shown in Fig. 2(a) can be written as

$$F(p_i,q) = \frac{1}{Z}F_{\mathrm{BH}}(p_i,q)\sum_b \Phi_b(p_2,q), \quad (21)$$

with

$$\Phi_b(p_2,q) = \int d^3r \psi^*_{\mathbf{p}_2}(r)\psi_b(r)\exp[-i(\mathbf{q}\cdot\mathbf{r})]. \quad (22)$$

Here $\psi_{\mathbf{p}_2}$ is the wave function of the outgoing electron with asymptotical momentum $\mathbf{p}_2$ and b denotes the bound electron. Since $p_2 \sim \eta$, the interactions between the outgoing electron and the residual ion cannot be treated perturbatively.

Thus we can write

$$d\sigma = \frac{1}{Z^2} d\sigma_{\mathrm{BH}} \sum_b |\Phi_b(p_2,q)|^2 \frac{d^3p_2}{(2\pi)^3}. \quad (23)$$

The Bethe-Heitler distribution

$$d\sigma_{\mathrm{BH}} = R d\Gamma', \quad d\Gamma' = dE_p p_{et} dp_{et} p_{pt} dp_{pt} d\varphi,$$

with [2,3]

$$R = \frac{8\alpha r_e^2 Z^2 E_e E_p}{\pi q^4 \omega^3} H \quad (24)$$

and

$$H = -\frac{\delta_-^2}{(1+\delta_-^2)^2} - \frac{\delta_+^2}{(1+\delta_+^2)^2} + \frac{\omega^2}{2E_eE_p}\frac{\delta_-^2+\delta_+^2}{(1+\delta_-^2)(1+\delta_+^2)} + \left(\frac{E_e}{E_p}+\frac{E_p}{E_e}\right)\frac{\delta_-\delta_+\cos\varphi}{(1+\delta_-^2)(1+\delta_+^2)} \quad (25)$$

(here we denoted $\delta_- = p_{et}/m$, $\delta_+ = p_{pt}/m$) should be evaluated for $p_{it} \sim m$, as in the Bethe-Heitler case, but now we also need $q \sim \eta_b \ll m$. This means that $|p_{et} - p_{pt}| \sim \eta_b \ll p_{et,pt}$ and $|\pi - \varphi| \sim \eta_b/m \ll 1$. Introducing variables q and $t = (p_{et} - p_{pt})/q$ $(-1 \leqslant t \leqslant 1)$, we can present Eq. (25) in the form

$$H = \frac{q^2}{m^2(1+\delta_+^2)^2}\left(\Lambda + \frac{4\delta_+^2 t^2}{(1+\delta_+^2)^2}\right), \quad (26)$$

with

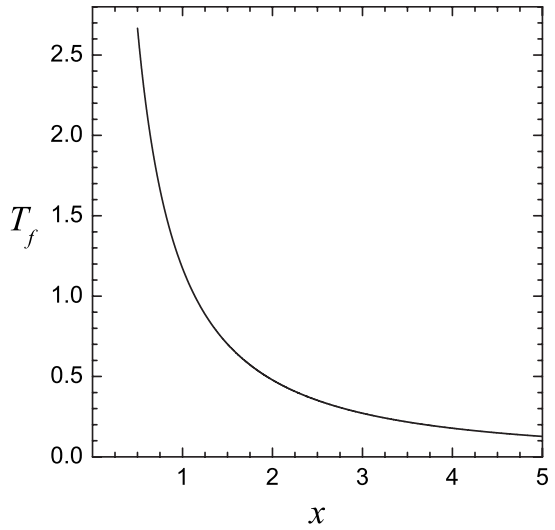

FIG. 3. The function $T_f(x)$ describing energy distributions of fast electrons as defined by Eq. (19), with x standing for the electron kinetic energy in units of the electron mass.

$$\Lambda = \frac{E_e^2 + E_p^2}{2E_eE_p} \quad (E_e = \omega - E_p), \quad (27)$$

while the phase volume in Eq. (23) becomes

$$d\Gamma' = dE_p p_{pt}^2 dp_{pt} \frac{dt}{2(1-t^2)^{1/2}} dq^2. \quad (28)$$

After integration over the positron variables and over t we find

$$d\sigma = \frac{14}{9}\alpha r_e^2 \sum_b |\Phi_b(p_2,q)|^2 \frac{dq^2}{q^2}\frac{d^3p_2}{(2\pi)^3}. \quad (29)$$

The factors $\Phi_b(p_2,q)$ turn to zero at $q=0$ due to orthogonality of the wave functions involved. Thus $\Phi_b(p_2,q)$ contains q as a factor at $q \to 0$, and the integral over q on the right-hand side (RHS) of Eq. (29) provides a finite value.

The factors $\Phi_b(p_2,q)$ have been computed for many cases in connection with the electron-atomic scattering. Here we present calculations with the nonrelativistic Coulomb functions. We shall provide results for K shell electrons. Thus the further results of this section are actually true for the ground states of relatively light [Eq. (2)] single-electron ions.

Straightforward calculations provide

$$|\Phi_K(p_2,q)|^2 = 2^8\pi N^2 \exp(2\xi\gamma) \times \frac{\eta^5[(q^2-(\mathbf{p}_2\cdot\mathbf{q}))^2 + \xi^2(\mathbf{p}_2\cdot\mathbf{q})^2]}{a^4|b|^2}. \quad (30)$$

Here $\eta = m\alpha Z$ is the averaged momentum of the K electron and

$$\xi = \frac{\eta}{p_2} = \sqrt{\frac{I}{\varepsilon_2}} \quad (31)$$

is the Sommerfeld parameter of interaction between the outgoing electron and the nucleus. The other notations in Eq. (30) are $a = (\mathbf{p}_2 - \mathbf{q})^2 + \eta^2$, $b = q^2 - (p_2 + i\eta)^2$, while $\gamma = \arg b = \arg(q^2 + \eta^2 - p_2^2 - 2i\eta p_2)$. The factor

$$N^2 = N^2(\pi\xi) = \frac{2\pi\xi}{1-\exp(-2\pi\xi)} \quad (32)$$

is the squared normalization factor of the outgoing electron wave function.

Presenting the phase volume of the outgoing electron as $d^3p_2/(2\pi)^3 = mp_2 d\varepsilon_2 d\Omega/(2\pi)^3$, we can carry out integration over the solid angle Ω

$$\int \frac{d\Omega}{(2\pi)^3}|\Phi_K(p_2,q)|^2 = q^2 X(p_2,q), \quad X(p_2,q) = \frac{2^7}{3\pi}N^2\exp(2\xi\gamma)\frac{u(p_2,q)}{v(p_2,q)}. \quad (33)$$

Here $u(p_2,q) = \eta^5(p_2^2 + 3q^2 + \eta^2)$ and $v(p_2,q) = [(q^2 - p_2^2)^2 + 2\eta^2(q^2 + p_2^2) + \eta^4]^3$. Combining Eqs. (29) and (33) we can write

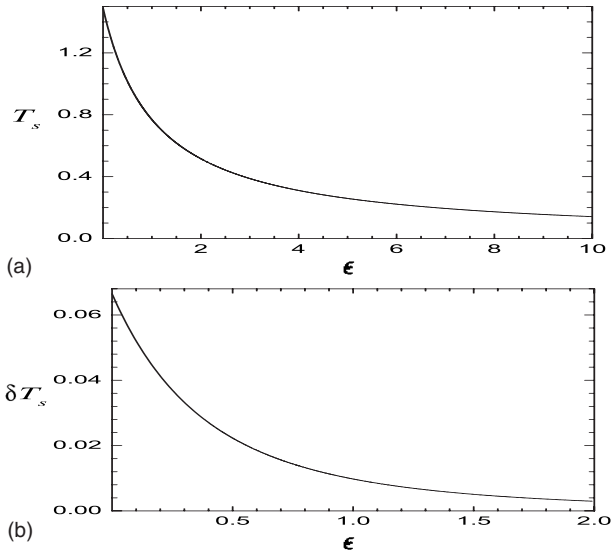

FIG. 4. (a) The function $T_s(\epsilon)$ describing energy distributions of slow electrons as defined by Eq. (39), with ϵ standing for the electron kinetic energy in units of the ionization potential. (b) The energy dependence of the difference $\delta T_s = \tilde{T}_s - T_s$ between approximate function $\tilde{T}_s$ defined by Eq. (51) and the function T_s.

$$\frac{d\sigma}{d\varepsilon_2} = \frac{14}{9}\alpha r_e^2 m p_2 \int dq^2 X(p_2,q). \tag{34}$$

Introducing

$$\epsilon = \frac{\varepsilon_2}{I} = \xi^{-2}, \tag{35}$$

we find

$$\frac{d\sigma}{d\epsilon} = \frac{14}{9}\alpha r_e^2 K(\epsilon), \tag{36}$$

with

$$K(\epsilon) = \frac{2^6}{3\pi\xi} N^2 \int_0^\infty dx \frac{e^{-2\gamma_1/\sqrt{\epsilon}}(\mu + 3x)}{(x^2 + 2\nu x + \mu^2)^3}, \tag{37}$$

with $\mu = 1+\epsilon$, $\nu = 1-\epsilon$, and $\gamma_1 = \arg(x+\nu+2i\sqrt{\epsilon})$.

Thus the energy distribution can be presented as

$$\frac{d\sigma}{d\varepsilon_2} = \frac{\alpha r_e^2}{I} T_s(\epsilon) \tag{38}$$

(the lower index s comes from "slow") with $I = m(\alpha Z)^2/2$ being the K-electron binding energy, and

$$T_s(\epsilon) = \frac{14}{9} K(\epsilon). \tag{39}$$

The function $T_s(\epsilon)$ is shown in Fig. 4.

Since $N^2 \sim \epsilon^{-1/2}$ at $\epsilon \to 0$—see Eq. (32)—we find a nonzero value for

$$K(0) = 1 - \frac{7}{3}\exp(-4) \approx 0.957. \tag{40}$$

Using Eq. (32) one can present Eq. (37) also as

$$K(\epsilon) = \frac{2^7}{3(1 - e^{-2\pi/\sqrt{\epsilon}})} J(\epsilon), \quad J(\epsilon) = \int_0^\infty dx \frac{e^{-2\gamma_1/\sqrt{\epsilon}}(\mu + 3x)}{(x^2 + 2\nu x + \mu^2)^3}. \tag{41}$$

At $\varepsilon_2 \gg I$ Eq. (31) provides $\xi \ll 1$, and thus $\epsilon \gg 1$. The lowest order of expansion in powers of ξ, corresponding to a plane wave description of the outgoing electron leads to

$$K(\epsilon) = \frac{1}{\epsilon}. \tag{42}$$

Thus for $I \ll \varepsilon_2 \ll m$

$$T_s(\epsilon) = \frac{14}{9}\frac{1}{\epsilon}, \tag{43}$$

in agreement with the nonrelativistic limit $\varepsilon_2 \ll m$ of Eq. (18)—see Eq. (20).

We see that the lowest order expansion in powers of ξ of the RHS of Eq. (37) leads to the same result as provided by the nonrelativistic limit of Eq. (18). On the other hand, the function K depends on ξ in terms of parameter $\epsilon = \xi^{-2}$, containing also explicit dependence on the parameter $\pi\xi$. The latter thus includes the terms which are linear in ξ, containing also a numerically large coefficient. We show, however, that in our case dependence on $\pi\xi$ cancels out at least in the lowest order terms of ξ^2 expansion.

On the RHS of Eq. (37) dependence on $\pi\xi$ is contained explicitly in normalization factor N^2 determined by Eq. (32). Such dependence comes also from the exponential factor of the integrand of $J(\epsilon)$ determined by Eq. (41). Since

$$J(\epsilon) = \int_{1-\epsilon}^\infty dy (4\epsilon + 3y - 2) \frac{\exp(-2\gamma_1/\sqrt{\epsilon})}{(y^2 + 4\epsilon)^3}$$

(we denoted $y = x - \epsilon + 1$) is dominated by $y \approx 2\sqrt{\epsilon}$ we can replace it by

$$J_1(\epsilon) = \int_{-\infty}^\infty dy (4\epsilon + 3y - 2) \frac{\exp(-2\gamma_1/\sqrt{\epsilon})}{(y^2 + 4\epsilon)^3}, \tag{44}$$

making the relative error of the order $\xi^5 \ll 1$. Since

$$\gamma_1 = \arctan\left(\frac{2}{y\xi}\right) \quad \text{at } y > 0, \quad \gamma_1 = \pi - \arctan\left(\frac{2}{|y\xi|}\right) \quad \text{at } y < 0 \tag{45}$$

($\xi = \epsilon^{-1/2}$), while for any $x > 0$

$$\arctan x = \frac{\pi}{2} - \arctan x^{-1}, \tag{46}$$

we can write

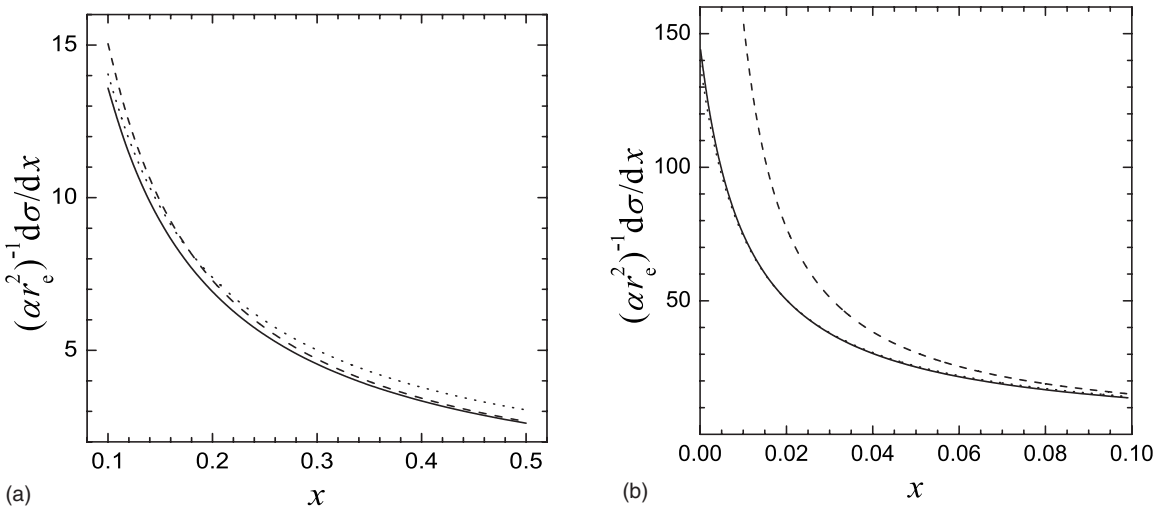

FIG. 5. Matching of the two regions of the electron spectrum for the characteristic case $Z=20$. Dashed line shows the function $T_f(x)$ defined by Eq. (19), calculated for the fast electrons with $x=\varepsilon_2/m$. Dotted line shows the function $(m/I)T_s(mx/I)$, describing distribution of slow electrons. Solid line shows the function $\tilde{T}_f(x)$ defined by Eq. (53). In (b) we show the lower part of the spectrum in more detail [the energy value $\varepsilon_2=m(\alpha Z)^2/2=5.4$ keV corresponds to $x\approx 1.07\times 10^{-2}$].

$$J_1(\epsilon)=\exp(-\pi\xi)\int_0^\infty dy(4\epsilon+3y-2)\frac{\exp[2\xi\arctan(y\xi/2)]}{(y^2+4\epsilon)^3}. \tag{47}$$

Integral (47) can be evaluated analytically

$$J_1(\epsilon)=\frac{3}{2^6}\exp(-\pi\xi)\sinh(\pi\xi)\frac{1}{\epsilon+1}. \tag{48}$$

Using Eq. (31) we find that the total dependence of the energy distribution on parameter $\pi\xi$ cancels out. The limiting Eq. (42) for $\epsilon\gg 1$ can be written as

$$K(\epsilon)=\frac{1}{\epsilon+1}[1+O(\epsilon^{-5/2})]. \tag{49}$$

Being more rigorous we should replace $1/(1+\epsilon)$ by $1-\epsilon+\epsilon^2$.

Thus several next to leading order corrections to the high energy limit of the function $T_s(\epsilon)$ can be included by a simple factor

$$g(\epsilon)=\frac{\epsilon}{\epsilon+1}. \tag{50}$$

As one can see from Fig. 4(b) the function

$$\tilde{T}_s(\epsilon)=\frac{14}{9}\frac{1}{\epsilon+1} \tag{51}$$

approximates the function (39) well enough even at ε_2 close to zero. The largest relative deviation between the RHS of Eqs. (39) and (51) takes place at $\epsilon_2=0$, being about 4%.

V. MATCHING OF THE TWO REGIONS

The function T_f determined by Eq. (19) describes the energy distribution at $\varepsilon_2\gg I$ and does not include corrections of the order ϵ^{-1}. On the other hand, the function T_s (39) describes the energy distribution at $\varepsilon_2\ll m$ since the outgoing electron is treated nonrelativistically.

One should investigate if there is energy region

$$I\ll\varepsilon_2\ll m, \tag{52}$$

where both equations describe the energy distribution, i.e., if there is a region where corrections to both distributions are small. The actual analysis show that such a region exists. In Fig. 5 we show the functions $T_{f,s}$ for characteristic value $Z=20$. The two descriptions overlap for the energies ε_2/m between 0.1 and 0.2, i.e., for the energies $\varepsilon_2\sim m\alpha Z$ ($\alpha Z=0.146$ for $Z=20$).

Taking into account the Coulomb corrections to the wave function of the outgoing electron in the distribution T_f one can expand the consistency of the two descriptions to lower energy values. As we saw in the preceding section, the lowest order Coulomb corrections can be taken into account by the factor g given by Eq. (50), i.e., by changing $T_f(x)$ to

$$\tilde{T}_f(\varepsilon_2)=T_f(x)g(\epsilon). \tag{53}$$

The function $\tilde{T}_f(\varepsilon_2)$ is also shown in Fig. 5.

VI. TOTAL CROSS SECTION

Now we must calculate the total cross section. Following analysis of the preceding section, we present

$$\sigma=\sigma_s+\sigma_f, \tag{54}$$

with the two terms on the RHS corresponding to slow and fast ionized electrons

$$\sigma_s = \frac{\alpha r_e^2}{I}\int_0^{\varepsilon_0} d\varepsilon_2 T_s\left(\frac{\varepsilon_2}{I}\right), \quad \sigma_f = \frac{\alpha r_e^2}{m}\int_{\varepsilon_0}^{\omega} d\varepsilon_2 T_f\left(\frac{\varepsilon_2}{m}\right), \tag{55}$$

with ε_0 belonging to the interval determined by Eq. (52). Since $T_f(x)$ drops as $\ln x/x^2$ at $x\to\infty$—see Eq. (19)—the contribution σ_f has a finite value at $\omega\to\infty$. Using Eqs. (18) and (42) we find

$$\sigma_s = \frac{14}{9}\alpha r_e^2\left(\ln\frac{\varepsilon_0}{I} + c_s\right), \quad \sigma_f = \frac{14}{9}\alpha r_e^2\left(\ln\frac{m}{\varepsilon_0} + c_f\right). \tag{56}$$

The contributions c_s and c_f come from the regions $\varepsilon_2 \sim I$ and $\varepsilon_2 \sim m$ correspondingly. Thus the total cross section can be written as

$$\sigma = \frac{14}{9}\alpha r_e^2\left(\ln\frac{m}{I} + C\right), \tag{57}$$

with $C=c_s+c_f$. In this approach C can exhibit a weak dependence on Z.

Note that the low energy contribution to c_s can be calculated as

$$c_s = \int_0^{\infty} d\epsilon[T_s(\epsilon) - \tilde{T}_s(\epsilon)], \tag{58}$$

with the functions T_s and $\tilde{T}_s$ being determined by Eqs. (39) and (51). The integral is saturated by $\epsilon \lesssim 1$, providing the value $c_s=-0.027$.

The presentation (57) for the cross section can be obtained by noting that the function (53) approximates the energy distribution well enough. The largest deviations from the exact curve are of the order of several percent, taking place at $\varepsilon_2 \lesssim I$. Using Eq. (20) we find that $\tilde{T}_f(\varepsilon_2)=(14/9)\times[m/(\varepsilon_2+I)]$ at $\varepsilon_2 \ll m$, providing the logarithmic term on the RHS of Eq. (57). Since at $\varepsilon_2 \sim I$ we can put $\tilde{T}_f(\varepsilon_2)=(m/I)\tilde{T}_s(\epsilon)$, parameter c_s is determined by Eq. (58). The actual numerical calculations employing the function $\tilde{T}_f(\varepsilon_2)$ provide values of C changing from 1.23 for $Z=1$ to 1.31 for $Z=50$. Note that the integral over large energies converges slowly due to a rather slow drop of the function $T_f(x)$—see Eq. (18). For characteristic value $Z=20$ we obtain $c_f=C-c_s=1.27$, putting $\omega=\infty$ as the upper limit of the second integral on the RHS of Eq. (55). However, assuming the upper limits of integration to be 5 or 10 m we find the values of c_f to be 0.67 and 0.91 correspondingly.

For the ground state of a not very heavy [Eq. (2)] single-electron ion $I=m(\alpha Z)^2/2$ and Eq. (57) can be written as

$$\sigma = \frac{14}{9}\alpha r_e^2\left(\ln\frac{2}{(\alpha Z)^2} + C\right). \tag{59}$$

If the parameter $(\alpha Z)^2$ is not treated as a small one, one should use relativistic Coulomb functions for all the electrons and positron. It is known [11] that the ultrarelativistic particles of the e^-e^+ pair can be described by the Furry-Sommerfeld-Maue (FSM) functions [12] which provide the relative accuracy $(\alpha Z)^2/\ell$ with ℓ standing for the orbital momenta. Since the pair transfers momentum $q \sim m$ to the nucleus or to the outgoing electron the values of $\ell \sim p_i/q \sim \omega/m$ are important. Thus corrections to FSM functions can be neglected. The calculation for the pair creation in the field of the nucleus [11] resulted in an additional contribution $f(Z)$ to the cross section, which does not depend on the photon energy, and can be presented as an $(\alpha Z)^2$ series. In our process the ultrarelativistic particles of the pair can be considered in a similar way, providing the same contribution $f(Z)$ to the cross section.

However, the bound electron and the ionized electron at $\varepsilon_2 \sim m$ should be described by totally relativistic Coulomb functions at $\alpha Z \sim 1$. One can employ the presentation [13] in which relativistic functions are expressed in terms of an $(\alpha Z)^2$ series with the FSM functions as zero order terms. Hence in the case $\alpha Z \sim 1$ the cross section can be written as

$$\sigma = \frac{14}{9}\alpha r_e^2\left(\ln\frac{m}{I} + C_R\right), \tag{60}$$

with $C_R=C+(\alpha Z)^2\delta C$, while δC can be presented as a certain $(\alpha Z)^2$ series.

Until now we considered a single electron ion. Turning to the case of an atom containing Z electrons or of an ion containing n_e electrons one can see that for any bound electron the structure of the cross section (60) is similar to that of the single electron case. The contribution c_f caused by large energies $\varepsilon_2 \sim m$ is the same for all the electrons. We saw the contribution c_s to be numerically small for K electrons. Since the other electrons are less bound, it is still smaller for them and can be neglected. Thus we can write for a bound electron with the binding energy I_b,

$$\sigma = \frac{14}{9}\alpha r_e^2\left(\ln\frac{m}{I_b} + C\right), \tag{61}$$

with $C \approx 1.3$.

Note that our cross section reaches a constant value at $\omega\to\infty$. On the other hand, the cross section of pair creation in the field of the nucleus [2] and that on a free electron [6,7] increase as $\ln\omega$ in this limit. This happens because the logarithmic terms are caused by integration over momentum transferred q in the former case and over the momentum of outgoing electron p_2 in the latter case. In both cases the lower limits of integration are of the order m^2/ω, causing the terms $\ln\omega$ in the cross sections. In our case the effects of the binding are important at the lower limits and we obtain $\ln 1/(\alpha Z)^2$ instead.

In [14] ionization of internal shells of silver and gold atoms in coincidence with pair creation was measured for 1 GeV photons. Using Eq. (61) we find the cross sections for ionization of the K shells to be 7.8 mb in Ag and 5.9 mb in Au. In the latter case $Z=79$ and the errors can be about 30%. The experimental results are 18 ± 6 mb for Ag and 8.3 ± 6.2 mb for Au. Our result for ionization of the L shell in Au is 37 mb, while the experiment provides 116 ± 76 mb. Thus our calculations underestimate the experimental data for silver, being in agreement with the results for gold. In general, our approach becomes less accurate with increasing

of the nuclear charge Z. A somewhat better agreement with experimental results for gold is likely to be due to the larger experimental uncertainties in this case.

Note that we considered ionization of atoms accompanied by pair creation in the field of the latter. For not very large Z, i.e., for $(\alpha Z)^2 \ll 1$ we found the field of the bound electrons to be more important, while interactions with the nucleus provided correction of the order $(\alpha Z)^2$. The authors of paper [1] separated the process into two, considering separately the contributions with interactions between the particles of the created pair with the nucleus being neglected and being included in a semiclasssical way. Now we can compare our results with the results of [1] where they are shown in Figs. 3 and 4. In our case the cross section drops slowly with Z in agreement with [1]. The values of the cross sections are also close in the two approaches, with the relative difference being about 20–30 %. Unfortunately, the logarithmic scale used in the figures of [1] does not permit us to compare the results in some detail. For the case $Z=20$ considered in [1] both approaches show the cross section accompanied by pair creation in the field of the nucleus to be much smaller than that in the field of the bound electrons. It was found in [1] that at large Z the former mechanism dominates in formation of ions. We did not consider the point, noting however that there is no consistent QED calculation yet and the role of interference of the two mechanisms is still obscure.

Now we find the values of the photon energy ω for which the considered process is the main mechanism of formation ions. We must compare the cross section of our process to the asymptotics of photoionization and to that of the Compton scattering on the bound electrons. For small and moderate values of Z the cross section of the latter process is larger than that of the former one at $\omega \gg m$. The total cross section of the high energy Compton scattering on a bound electron is equal to that on a free electron [15]. The asymptotics of the latter is

$$\sigma_C = \pi r_e^2 \frac{\ln(2y) + 1/2}{y},$$

with $y=\omega/m$. The cross section of our process becomes larger than σ_C at certain $\omega=\omega_0$. In Fig. 6, we show Z dependence of ω_0 for the K electrons of single electron ions and of atoms. The value for hydrogen $\omega_0=73.6$ MeV is the smallest one. For the external electrons the values of ω_0 become still smaller due to the small values of the binding energies. For example, the binding energies of $3s$ and $4s$ electrons in Na and K are 4.9 and 4.1 eV correspondingly [16], providing the values $\omega_0=65.6$ MeV and $\omega_0=66.7$ MeV.

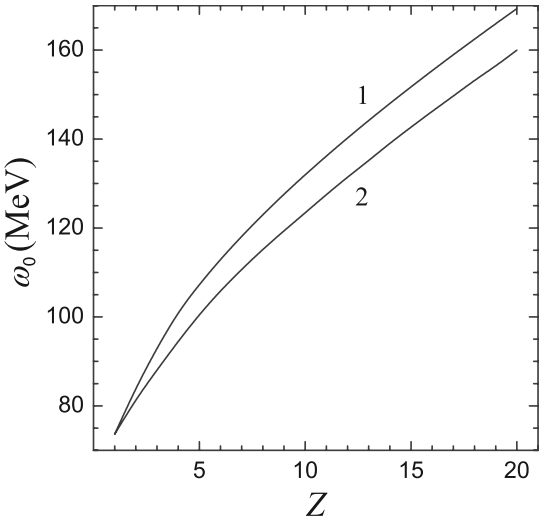

FIG. 6. Dependence of the photon energy ω_0 on the value of the nuclear charge Z. At $\omega > \omega_0$ the ionization accompanied by creation of e^-e^+ pairs is the dominant mechanism of the K shell ionization. Curve 1 is for the single-electron ions; curve 2 is for atoms with Z electrons.

VII. SUMMARY

We analyzed formation of ions by high-energy photons accompanied by creation of e^-e^+ pairs. We calculated the energy distributions $d\sigma/d\varepsilon$ for creation of ion and a continuum electron with kinetic energy $\varepsilon \ll \omega$. We showed that the slow electrons with ε being of the order of the binding energies I_b and the fast electrons with the energies $\varepsilon \gg I$ need separate treatment. We carried out matching of the two regions and found analytical formula (53), which approximates the whole spectrum of the outgoing electrons.

We integrated the energy distributions and found expressions (59) and (61) describing the cross sections for the ionization of single-electron ions and of any state in a many-electron atom. We showed that the high energy asymptotics of the cross sections does not depend on the photon energy. We found the values of the photon energies ω_0 for which ionization accompanied by pair creation becomes the dominative mechanism for formation of ions. The Z dependence of ω_0 for K electrons is shown in Fig. 6. The value of ω_0 appeared to be about 74 MeV in hydrogen, increasing with Z, and being somewhat smaller for loosely bound external electrons of heavier atoms.

We carried out calculations for not very heavy atoms—see Eq. (2). The approach can be generalized for the case $\alpha Z \sim 1$ as well.

Note that a related problem of the influence of atomic electrons on the pair creation was considered in [17,18]. The authors focused on modification of characteristics of the created pair by atomic field. That is why they used some additional approximations in the description of atomic electrons. However, the totally integrated cross section which includes all inelastic transitions, presented in [19] for the case of hydrogen ($\sigma=\alpha r_e^2 \times 19$), can be compared with our result $\sigma = \alpha r_e^2 \times 18$.

Our results are in good agreement with the estimations made in the pioneering paper [1]. As far as we know, the only related experiment was carried out in [14]. Our results are consistent with these data. There are still large errors in experimental and theoretical analysis. This should stimulate further development of both.

ACKNOWLEDGMENTS

The work was partially supported by the DFG Grant No. 436 RUS 113/822/0-1. The work of Kh.R. was supported by INTAS YS Grant No. 04-83-2674 and by Uzbek Academy of Sciences Grant No. 66-06. Four of us (E.G.D., A.I.M., I.A.M., and Kh.R.) acknowledge hospitality during our visits to the Justus-Liebig University of Giessen.

[1] D. C. Ionescu, A. H. Sorensen, and A. Belkacem, Phys. Rev. A **59**, 3527 (1999).
[2] H. A. Bethe and W. Heitler, Proc. R. Soc. London, Ser. A **146**, 83 (1934).
[3] V. B. Berestetskii, E. M. Lifshitz, and L. P. Pitaevskii, *Quantum Electrodynamics* (Pergamon Press, New York, 1989).
[4] H. A. Bethe in *Handbuch der Physik*, vol. 24/1 (Springer, Berlin, 1933).
[5] E. G. Drukarev, Proceedings of 38th Winter PNPI School (in English), (SPb, PNPI, 2004), p. 340; e-print physics/0406048; M. Ya. Amusia, E. G. Drukarev, and V. B. Mandelzweig, Phys. Scr. **72**, C22 (2005).
[6] A. Borsellino, Nuovo Cimento **4**, 112 (1947).
[7] V. I. Baier, V. S. Fadin, and V. A. Khose, Sov. Phys. JETP **23**, 104 (1966).
[8] K. J. Mork, Phys. Rev. **160**, 1065 (1967).
[9] J. W. Motz, H. A. Olsen, and H. W. Koch, Rev. Mod. Phys. **41**, 581 (1969).
[10] E. Haug, Z. Naturforsch. A **30A**, 1099 (1975).
[11] H. A. Bethe and L. C. Maximon, Phys. Rev. **93**, 768 (1954); H. Davies, H. A. Bethe, and L. C. Maximon, *ibid.* **93**, 788 (1954).
[12] W. H. Furry, Phys. Rev. **46**, 391 (1934); A. Sommerfeld and A. W. Maue, Ann. Phys. **22**, 629 (1935).
[13] V. G. Gorshkov, Sov. Phys. JETP **13**, 1037 (1961).
[14] D. Dauvergne, A. Belkacem, F. Barrue, J. P. Bocquet, H. Chevallier, B. Feinberg, R. Kirsch, J. C. Poizat, C. Ray, and D. Rebreyend, Phys. Rev. Lett. **90**, 153002 (2003).
[15] V. G. Gorshkov, A. I. Mikhailov, and S. G. Sherman, Sov. Phys. JETP **37**, 572 (1973).
[16] S. Fraga, J. Karwowski, and K. M. S. Saxena, *Handbook of Atomic Data* (Amsterdam, Elsevier, 1976).
[17] J. A. Wheeler and W. E. Lamb, Phys. Rev. **55**, 858 (1939); **101**, 1836 (1956).
[18] L. C. Maximon and H. A. Gimm, Phys. Rev. A **23**, 172 (1981).
[19] H. A. Olsen, *Applications in Quantum Electrodynamics*, Springer Tracts in Modern Physics Vol. 44 (Springer-Verlag, Heidelberg, 1968).